CONCURRENCY AND COMPUTATION: PRACTICE AND EXPERIENCE
Concurrency Computat.: Pract. Exper. 2014; **26**:2518–2529
Published online 21 July 2014 in Wiley Online Library (wileyonlinelibrary.com). DOI: 10.1002/cpe.3335

SPECIAL ISSUE PAPER

The power of circuit simulations for designing photonic integrated circuits

C. Arellano[1,*,†], S. F. Mingaleev[2], E. S. Sokolov[2] and A. Richter[1]

[1] *VPIphotonics GmbH, Carnotstr. 6, 10587 Berlin, Germany*
[2] *VPI Development Center, Chapaeva str. 5, 220034 Minsk, Belarus*

SUMMARY

The emerging of circuit-level simulators for photonic integrated circuits (PICs) is driven by recent developments in technologies for integration of large-scale monolithic PICs in both, silicon and InP technologies. For that reason, powerful circuit-level simulators should be capable to model on the same circuit different types of sub-components performing photonic, electronic or opto-electronic, active or passive functions. In comparison with device-level simulations, the use of realistic circuit-level abstracted models facilitates rapid functional design without going into technological fabrication details and subsequent design flow. This accelerates the design process and decreases the number of runs to achieve the desired results. Detailed physical modeling remains limited to the design of some specific individual sub-elements. Large-scale PICs might comprise several thousands of elements. The circuit-level abstraction also ensures that the simulation speed to achieve a certain simulation accuracy decreases reasonably slowly with the total number of photonic components in the modeled PIC. In this work, we present our solution for modeling PICs in the framework of the circuit-level simulation tool *VPIcomponentMaker™Photonic Circuits* (Carnotstr. 6, 10587, Berlin, Germany, www.VPIphotonics.com). We demonstrate the combination of different simulation approaches in time domain, frequency domain and time-and-frequency domain for fast and accurate simulations. We discuss several diverse modeling benefits by means of application examples on silicon photonic PICs. Copyright © 2014 John Wiley & Sons, Ltd.

Received 10 June 2014; Revised ; Accepted 11 June 2014

KEY WORDS: photonic integrated circuits; circuit simulator; silicon photonics; electronic-photonic design

1. INTRODUCTION

For several years already, photonic integration technologies have been developed significantly, increasing the number of photonic components enclosed on a single chip as well as their complexities and functionalities. Nowadays, the number of elements per chip reaches several hundreds and is expected to be doubled every 2.5 years, following Moore's law in micro-electronics [1]. Powerful photonic circuit simulators are one of the key enablers to boost up such technologies.

In earlier works, we have already demonstrated the modeling of fully passive photonic integrated circuit (PICs), based on the description of sub-elements in terms of frequency-dependent scattering-matrices [2]. Later, we presented an original approach for efficient modeling of hybrid large-scale PICs containing active and clusters of passive sub-elements [3]. We named it time-and-frequency domain modeling (TFDM). In our most recent publication, we presented a functionality extension allowing the design of opto-electronic circuits containing linear electrical sub-elements as well [4].

*Correspondence to: C. Arellano, VPIphotonics GmbH, Carnotstr. 6, 10587 Berlin, Germany.
†E-mail: cristina.arellano@vpiphotonics.com

The circuit modeling approach presented in this work concerns the modeling and design of PICs that comprise elements of diverse nature as active semiconductor-based structures, passive waveguide elements and electrical elements.

2. PHOTONIC CIRCUIT SIMULATORS

Photonic circuit simulators should be able to handle a large diversity of complex models that account for a multitude of effective parameters, and nonlinear effects such as carrier dynamics, thermal and mechanical matters, or integrated electronic components. In addition, the bandwidth required to simulate optical signals is typically much larger compared with the electrical frequency ranges of interest. This gives way to sophisticated signal representations and modeling techniques increasing simulation efficiency.

The design complexity is addressed (to different degrees) in novel photonic circuit simulators [5–7] by techniques that are based on segmentation of the modeled PIC into building blocks, named PIC elements (Figure 1).

The PIC elements are described by transfer functions or physical models and several input/output or bidirectional ports that connect the elements in a circuit with each other. Signals are processed inside each PIC element in the frequency domain, for the case of linear passive elements, or in the time domain for active and nonlinear elements. Electric elements (EEs) work in a similar way; however, in that case, all EEs are assumed to be linear and processed in the frequency domain. The outgoing signals produced by each sub-element (or cluster of sub-elements) are passed to the adjacent ones as input signals. The way of passing signals between building blocks depends on the simulation domain that is employed.

3. COMPONENTS LIBRARY

The library of built-in components provides advanced models for designing active opto-electronic devices such lasers, SOAs, light-emitting diodes, vertical-cavity surface-emitting lasers (VCSELs), photo-detectors, and others. Active elements are best defined in time domain and support characteristics such as nonlinear effects, carrier dynamics, variable gain and absorption shape, and other

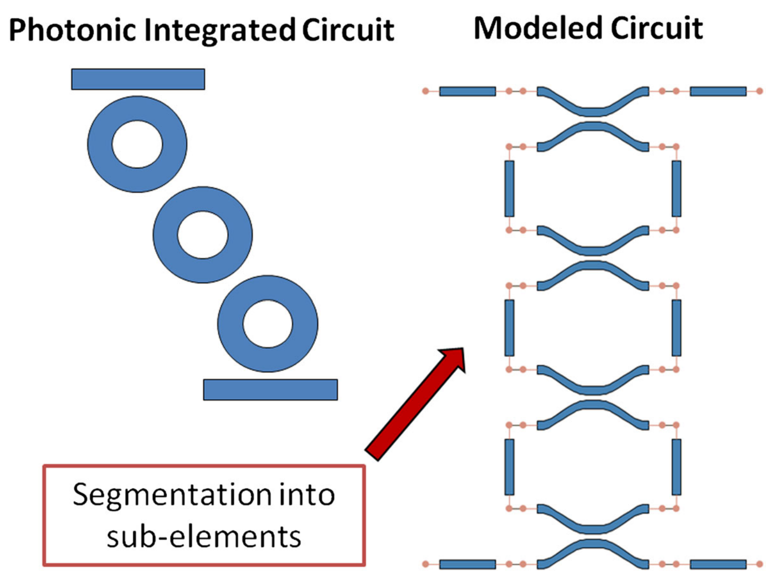

Figure 1. Simulation based on segmentation into photonic integrated circuit elements.

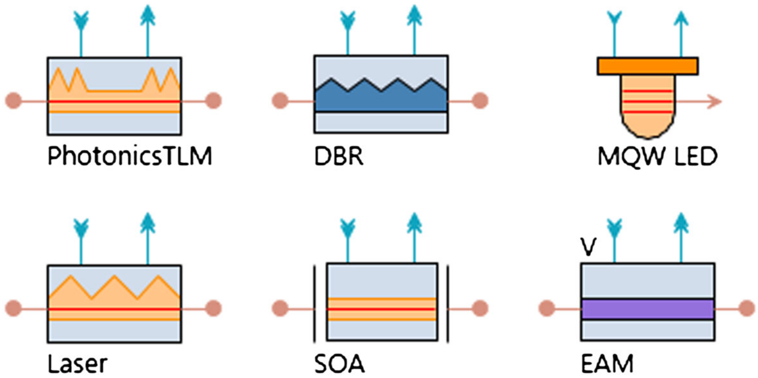

Figure 2. Examples of fundamental built-in active elements.

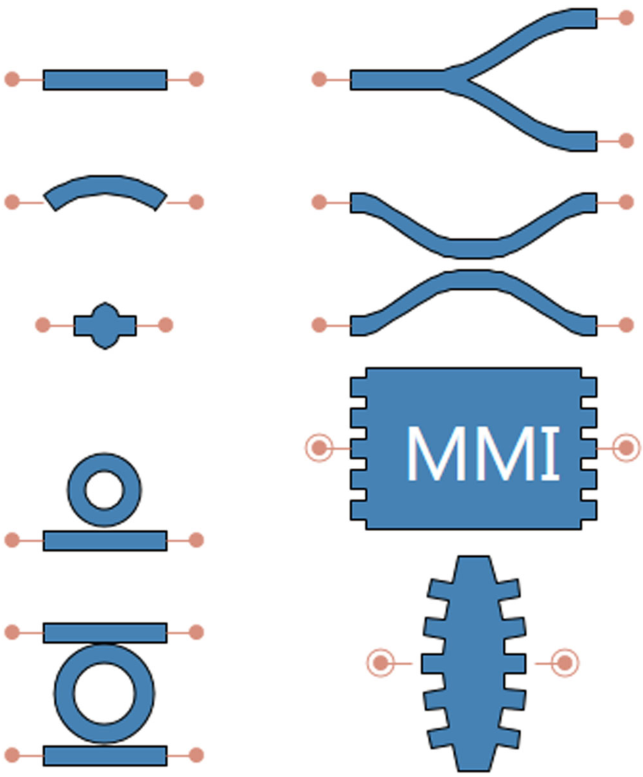

Figure 3. Examples of fundamental built-in passive elements.

properties (Figure 2). The library of passive PIC elements includes accurate analytical models for straight, bend or coupled waveguides, ring resonators and ring couplers, multi-mode interference (MMI)elements, star coupler, and junction elements. Such elements support frequency-dependent effective mode indices and attenuations (Figure 3). The collection of built-in electrical elements contains fundamental models for resistor, capacitor, inductor, mutual inductor, independent and dependent voltage, and current sources. DC, AC, and transient analysis might be carried out using EEs (Figure 4). Passive PIC elements and EEs are characterized by frequency-dependent transfer functions (S-matrix) between pairs of device ports. S-matrices are calculated from established theoretical models, measured models or by co-simulation with standard programming or scripting languages.

DOI: 10.1002/cpe

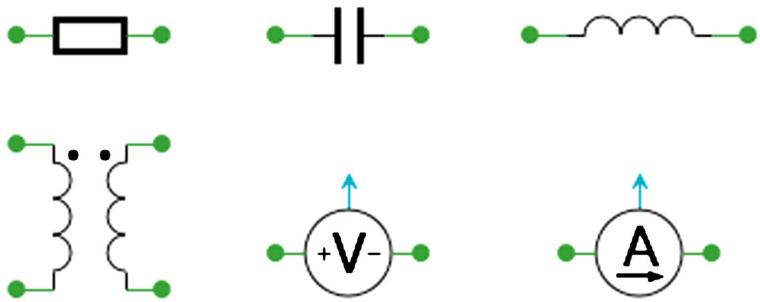

Figure 4. Examples of fundamental built-in electrical elements.

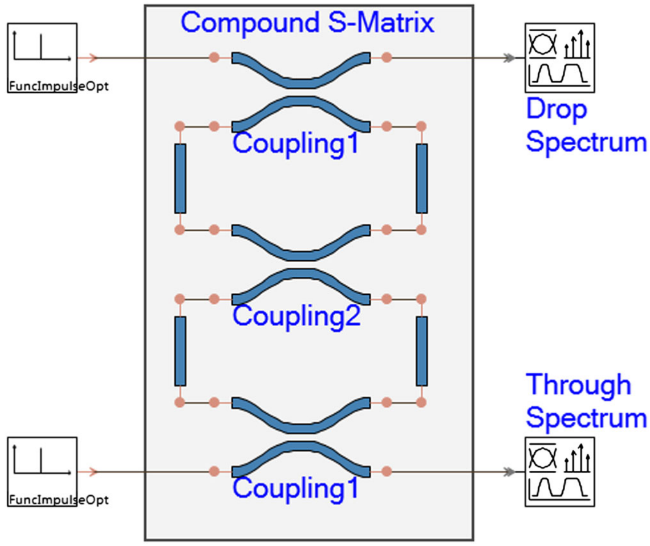

Figure 5. Schematic of the double-ring add-drop filter.

4. APPLICATION EXAMPLES

4.1. High-order micro-ring add-drop filter with flat passband

In this example, we consider a second-order add-drop filter consisting of two bus waveguides with two coupled rings between them (Figure 5). The setup can be straightforwardly modified to simulate an arbitrary specific number of rings between the bus waveguides. Properly designed, high-order micro-ring filters are characterized by improved passband characteristics and larger out-of-band signal rejection and are therefore very promising for complementary metal-oxid-semiconductor (CMOS) compatible implementation of wavelength-division multiplexing signal processing in a chip [8]. The example illustrates an efficient S-matrix domain technique for modeling passive PICs containing feedback loops. The simulation domain creates a compound S-matrix of the whole structure, which makes simulations very fast and accurate ($\sim$19,000 frequency points per second on a computer with 3.16 GHz Intel Core 2 Duo CPU).

The response after simulation shows a flattened resonant peak shape in both, drop and through spectra. The power coupling factor between the two rings induces changes in the passband shape. In the absence of attenuation, the maximally flat passband is achieved at `Coupling2 = 0.25*sqr(Coupling1)=0.01` (Figure 6), with `Coupling1 = 0.2`, the coupling between the ring and bus waveguide, what coincides with the results reported in [8].

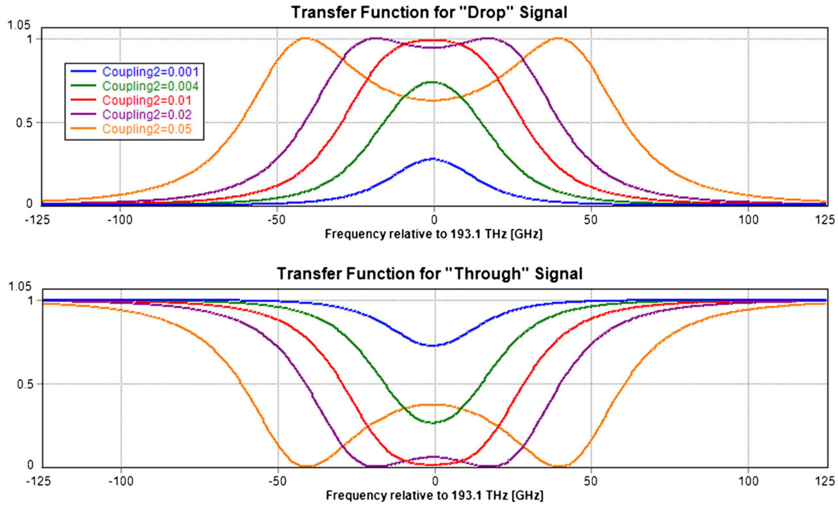

Figure 6. Simulation results: the ‘drop’ and ‘through’ transfer functions of the double-ring add-drop filter.

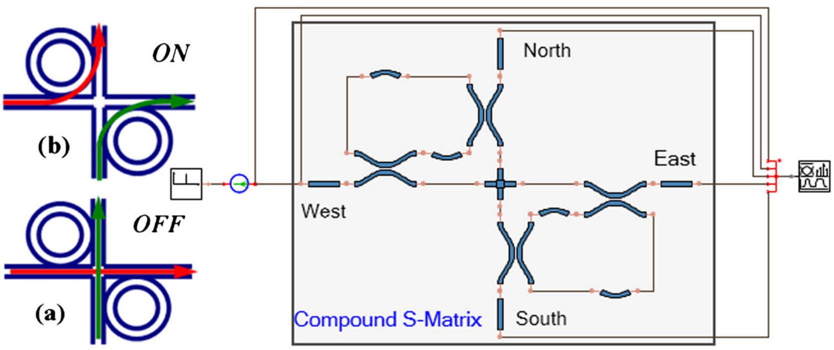

Figure 7. Schematic of photonic switching element.

4.2. Induced transparency in cross-coupled two-ring photonic switching element

The following case illustrates the functionality of a photonic switching element. The device consists of a waveguide intersection, positioned between two ring resonators [9] to control the routing of signals in optical networks and interconnections (Figure 7). The device exhibits in its ‘On’ state a complex effect, the so-called coupled-resonator-induced transparency (CRIT)—an all-optical analog to electromagnetically induced transparency, initially discovered for a system of two consecutive ring resonators.

Figure 8 shows the simulation results considering an ideal waveguide crossing and two ideal identical micro-rings, each coupled with both crossing waveguides (calculated with speed $\sim$6000 frequency points per second on a computer with 3.16 GHz Intel Core 2 Duo CPU). Both rings are designed to have resonances at frequency 193.1 THz. At this frequency, the modeled photonic switching element exhibits its ‘On’ state, while far away from this frequency, it exhibits ‘Off’ states. Notice the existence of an additional narrow transparency peak in the ‘West to East’ spectrum that slides over the broader resonance with the transmission phase. This is the transparency line caused by the CRIT effect (due to interference between two different light paths). It can be easily controlled by changing, for example, the temperature of the waveguide crossing area. The CRIT peak is affected by detuning the radii between two of the rings and by imperfections in waveguide crossings (reflections and crosstalk). Notice a splitting of the CRIT peak with such imperfections, caused also by additional light paths and the corresponding interference effects between them.

DOI: 10.1002/cpe

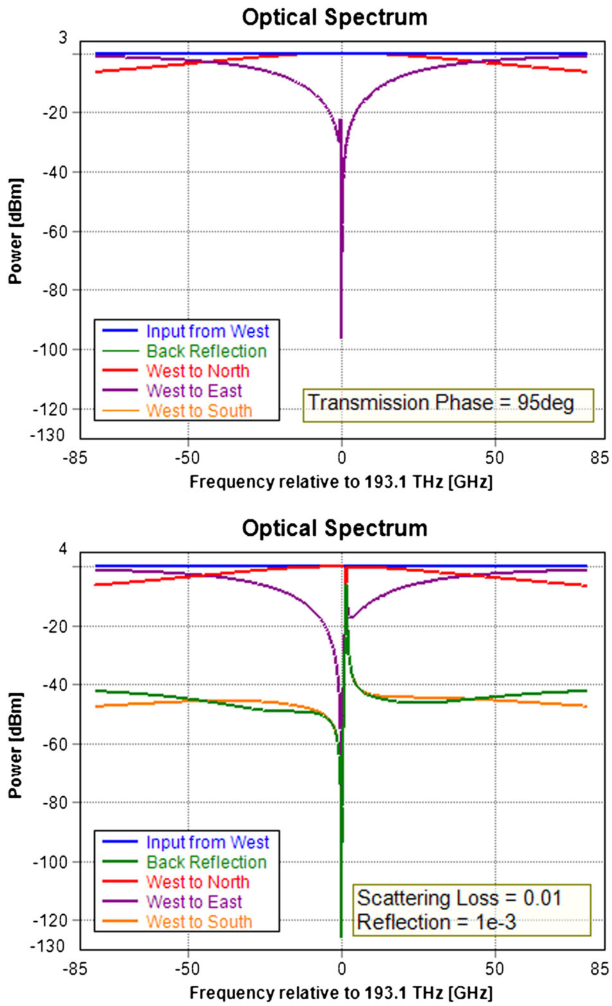

Figure 8. Simulation results: spectra at the different outputs for crossing element without attenuation and reflection (top); and for non-negligible attenuation and reflection (bottom).

4.3. Recirculating optical buffer

This example shows the implementation of an integrated recirculating optical buffer, based on the work reported in [10]. It comprises in addition three-ring add-drop filters for providing different optical buffer capacity at different channel wavelengths (16-bit delay at 194.1 THz and 8-bit delay for all neighboring channels). The PIC comprises a 2×2 gate matrix switch formed by two MMI splitters and four SOAs. The gate matrix is connected to the delay line loops. The electric circuit models an adaptive filter representing bandwidth limitations of in the driving circuit (Figure 9). We illustrate with this example how photonic, opto-electronic, and electrical sub-elements can be simulated together. The electric filter implements different transfer functions, depending on the values given to the resistances and capacitances. The transfer characteristic might be analyzed independently before introducing it in the full setup (Figure 10). The simulation technique we used for simulating this setup is the hybrid TFDM approach, described in [3]. In this technique, clusters of passive and electric sub-elements are identified (marked with 'f'), and equivalent S-matrices are calculated for each 'f-cluster'. The presence of active elements in this integrated circuit forces a time domain simulation. For this, equivalent FIR filters are calculated for each of the compounded S-matrices. Employing FIR filters of clusters of passive elements instead of designing an FIR filter for each single passive sub-element enables to provide much faster and more accurate results.

DOI: 10.1002/cpe

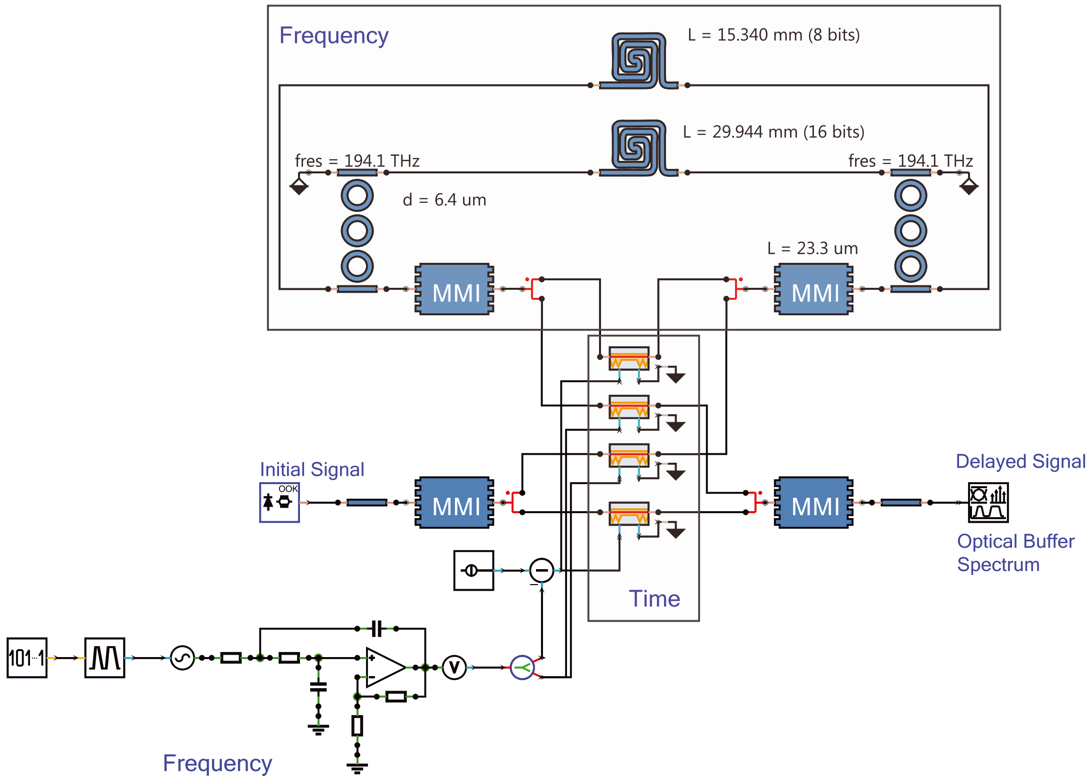

Figure 9. Schematic of recirculating optical buffer.

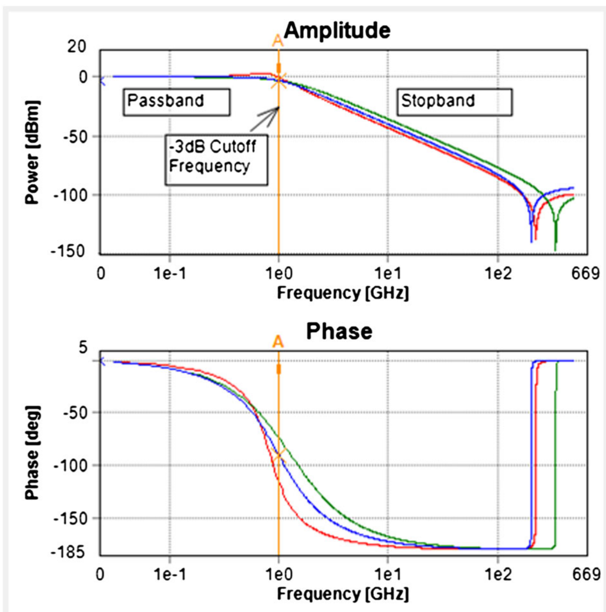

Figure 10. Transfer characteristics of the electrical filter for different values of electrical elements.

Figure 11 depicts the waveform for the 194.1 and 194.4 THz channels using sample rates of 640 GHz (right) and 2.56 THz (left). The latter results are calculated with the speed ~500 time steps per second on a computer with 3.16 GHz Intel Core 2 Duo CPU. The TFDM approach requires

DOI: 10.1002/cpe

Figure 11. Simulation results: delayed response of the two channels for two different simulation bandwidths.

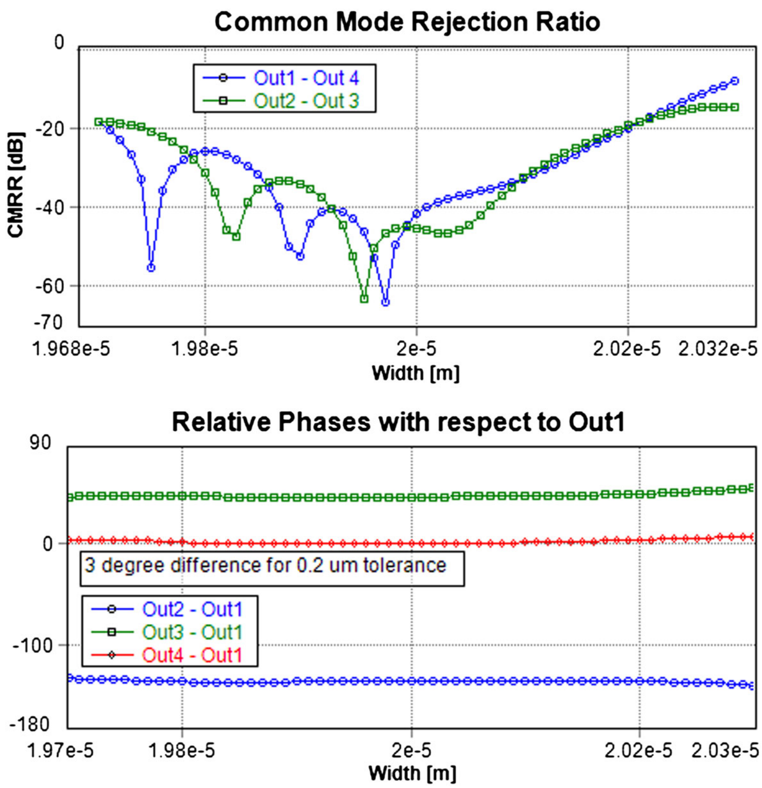

Figure 12. Simulations results: common-mode rejection ratio (CMRR) (top); and relative phase (bottom) at output ports.

much smaller sample rates in comparison with the standard time domain approach, which would need more than 56 THz for accurate simulation results.

4.4. Tolerances and optimization in MMIs

The device discussed now represents an implementation of a 90-degree optical hybrid made from 4×4 MMI coupler, which is modeled in VPIcomponentMaker Photonics Circuits by employing a self-imaging principle and guided mode propagation analysis (with simulation speed ∼5000 frequency points per second on a computer with 3.16 GHz Intel Core 2 Duo CPU). The 90-degree optical hybrid function is accomplished by illuminating only two of the MMI input ports; either the first and third or the second and fourth [11]. Tolerances of the fabrication process might lead to

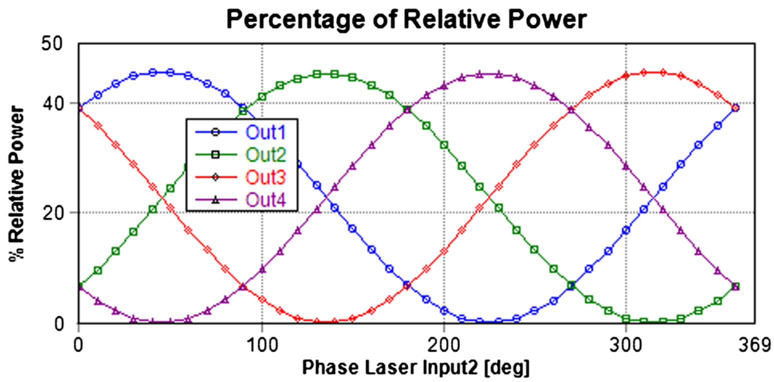

Figure 13. Simulation results: relative power at outputs.

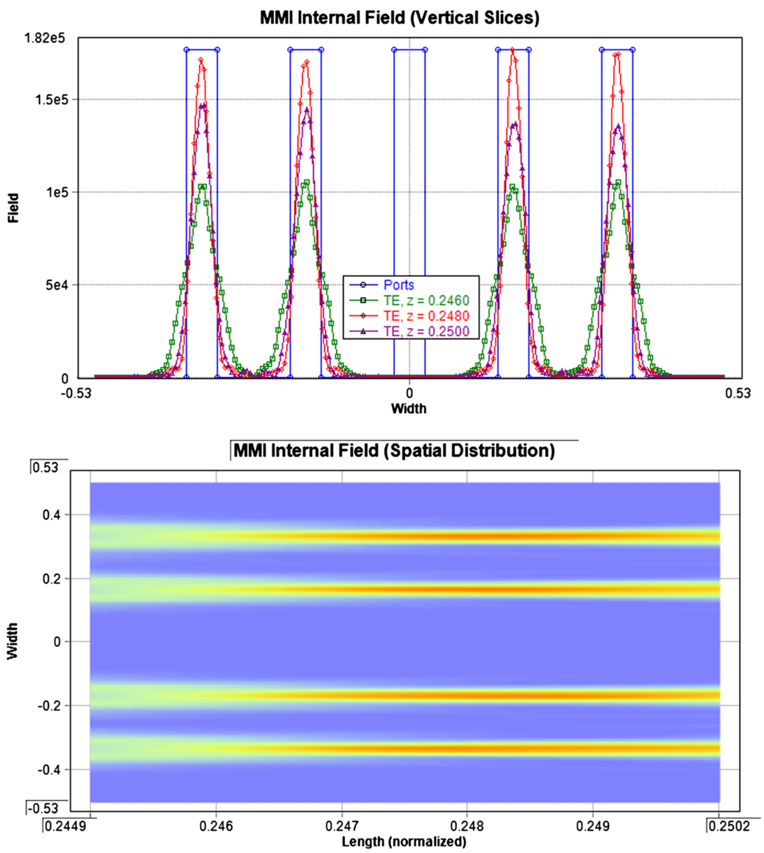

Figure 14. Simulation results: distribution of $E_x(x, z)$ field at different z-points of the multi-mode interference (MMI) (top) and in the (x, z)-plane (bottom), produced also by the VPIcomponentMaker Photonics Circuits.

wrong splitting operation, which are characterized in this setup by the phase relation and relative power at the outputs, and the common mode rejection ratio [12]. Variations from the nominal width of the MMI impact the relative output phases, what is not so critical. However, the common-mode rejection ratio is very sensitive to width variations and increases rapidly with increased deviations from the optimal width (Figure 12). The power distribution among the outputs is displayed in

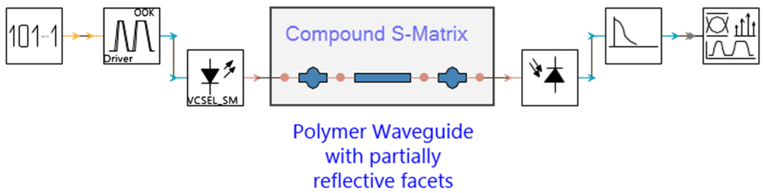

Figure 15. Schematic for chip-to-chip transmission.

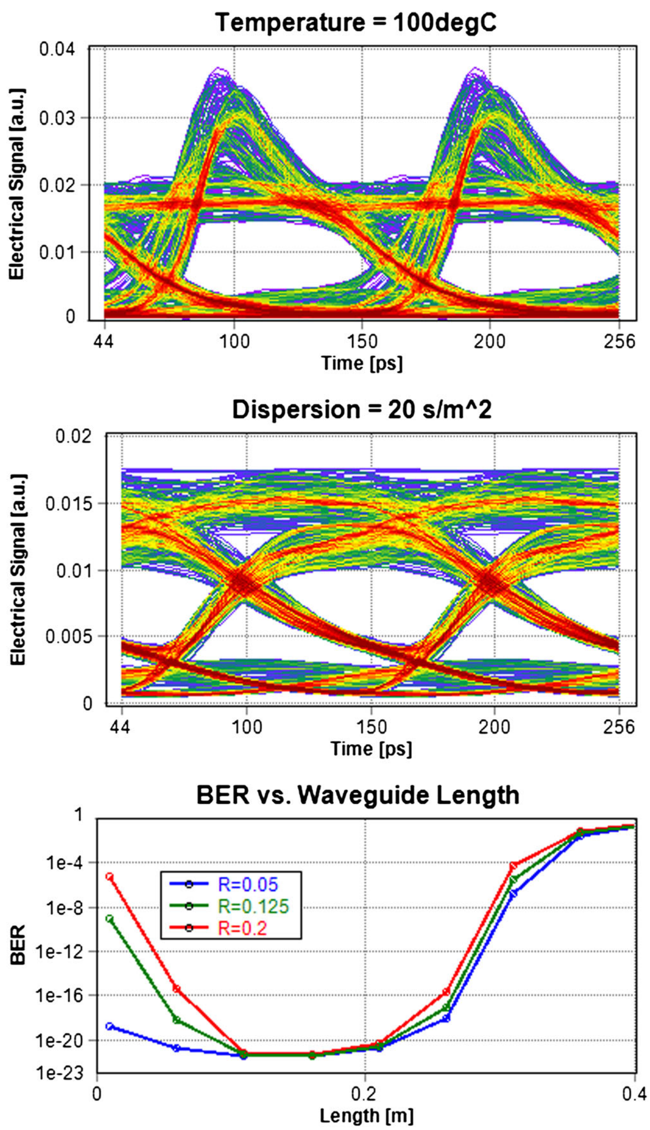

Figure 16. Simulation results (from top to bottom): eye diagram for an increased temperature of the vertical-cavity surface-emitting lasers; eye diagram considering dispersion in the polymer waveguide; and BER for different waveguide lengths.

DOI: 10.1002/cpe

Figure 13 for different input phases. The insertion loss can be also deducted from the relative power measurement. In an ideal case, the sum of the relative powers should be 100%.

In another example, we show the design and optimization of a 1×4 uniform splitter. To estimate the MMI length for which the output signals would be focused best, one should analyze the vicinity of the best focusing region. The field spatial distribution and the field profiles are displayed near the right end of the device on Figure 14, produced also by the VPIcomponentMaker Photonics Circuits. In this case, it is deduced that the best focusing of output fields is achieved for the normalized (in terms of characteristic beat length) length of the MMI of approximately 0.248.

4.5. Chip-to-chip transmission system

The application discussed now represents a possible realization of a chip-to-chip transmission system [13]. A VCSEL is used as transmitter source and a polymer waveguide to guide the signal through the chip board. At the other side of the waveguide, the signal data are received by a photo-detector. Such a simple structure could be scaled easily using several tens of parallel optical channels. Reflecting junction elements are used to couple the light perpendicularly to the chip waveguide (Figure 15).

We analyzed the impact of varied temperature on the dynamics of the VCSEL behavior and stress-induced birefringence. Dispersion in the waveguide might also distort severely the signal. Even though nearly zero polarization polymer waveguides can be designed for a certain wavelength [14], it can still be problematic because the transmission wavelength might shift because of temperature effects in the VCSEL. Additionally, possible Fabry–Perot resonances originated between the junctions might degrade the operation of the system. This is simulated by sweeping the length of the waveguide. For short lengths (could also be interpreted as waveguide attenuation), the BER increases because of the high power of the FP resonances. The lowest BER values are obtained for intermediate waveguide lengths. For longer lengths, the BER increases again because of the reduction of the waveguide attenuation. Thus, automatic parameter variations in this type of simulations allow finding the margin of waveguide length that represents the best implementations (see simulation results in Figure 16, calculated with speed ∼16,000 frequency points per second on a computer with 3.16 GHz Intel Core 2 Duo CPU).

5. SUMMARY

We have shown the power of circuit simulations for modeling photonic integrated circuits. Specifically, we have presented the professional design suite VPIcomponentMaker Photonic Circuits for the design and simulation of photonic integrated circuits comprising sub-elements of different nature. This has been demonstrated with application examples of photonic signal processing circuits, photonic elements, and systems.

REFERENCES

1. Moore GE. Cramming more components onto integrated circuits. *Electronics* 1965; **38**:114–117.
2. Arellano C, Mingaleev SF, Sokolov E, Koltchanov I, Richter A. Efficient design of photonic integrated circuits (PICs), *Paper Th.A4.1*, ICTON, 2011.
3. Arellano C, Mingaleev SF, Sokolov E, Koltchanov I, Richter A. Time-and-Frequency-Domain Modeling (TFDM) of Hybrid Photonic Integrated Circuits, *Paper 8265-19*, OPTO Photonics West, 2012.
4. Arellano C, Mingaleev SF, Sokolov RA. Modeling of Opto-Electronics in Complex Photonic Integrated Circuits, *Paper 8980-61*, OPTO Photonics West, 2014.
5. ASPIC. (Available from: http://www.aspicdesign.com) [accessed on 2014].
6. PICWave. (Available from: http://www.photond.com/products/picwave.htm)[accessed on 2014].
7. VPIcomponentMaker™Photonic Circuits. (Available from: http://vpiphotonics.com/CMPhotonicCircuits.php)[accessed on 2014].
8. Xiao S, Khan MH, Shen H, Qi M. Silicon-on-insulator microring add-drop filters with free spectral ranges over 30 nm. *Journal of Lightwave Technology* 2008; **26**(2):228–236.
9. Shacham A, Bergman K, Carloni LP. On the design of a photonic network-on-chip. *Proceedings of the 1st International Symposium Networks-on-Chip*, Princeton, NJ, 2007; 53–64.

DOI: 10.1002/cpe

10. Park H, Mack JP, Blumenthal DJ, Bowers JE. An integrated recirculating optical buffer. *Optics Express* 2008; **16**:11124.
11. Zimmermann L, Voigt K, Winzer G, Petermann, Weinert CM. C-band optical 90 deg-hybrids based on silicon-on-insulator 4x4 waveguide couplers. *PTL* 2009; **21**(3):143–145.
12. Pennings ECM, Deri RJ, Bhat R, Hayes TR, Andreadakis NC. Ultracompact, all-passive optical 90 deg-hybrid on InP using self-imaging. *PTL* 1993; **5**(6):701–703.
13. Schow C, Doany F, Kash J. Get on the optical bus. *IEEE Spectrum* 2010; **47**(9):32–56.
14. Chiang KS, Cheng SY, Chan HP, Liu Q, Lor KP, Chow CK. Realization of polarization-insensitive optical polymer waveguide devices. *International Journal of Microwave and Optical Technology* 2006; **1**(2):644–650.